Sharpness-enhanced ultrafast imaging by using a biased optical Kerr gate

Wenjiang Tan,[1] Pingping Zhan,[1] Jinhai Si,[1,*] Shichao Xu,[1] Junyi Tong,[2] Huailiang Xu,[3] and Xun Hou[1]

[1]*Key Laboratory for Physical Electronics and Devices of the Ministry of Education, Shannxi Key Lab of Information Photonic Technique, School of Electronic and information Engineering, Xi'an Jiaotong University, Xianning-xilu 28, Xi'an, 710049, China*

[2]*Departments of Applied Physics, Xi'an University of Technology, Xi'an 710048, China*

[3]*State Key Laboratory on Integrated Optoelectronics, College of Electronic Science and Engineering, Jilin University, 2699 Qianjin Street, Changchun 130012, China*

[*]*jinhaisi@mail.xjtu.edu.cn*

Abstract: We proposed a novel biased optical Kerr gated imaging (BOKGI) method for ultrafast imaging. The imaging performance of the BOKGI system has been investigated. Experimental results showed that by using the BOKGI, the high spatial frequency components of the detected object could be effectively retrieved, which are often filtered by the photo-induced soft aperture in a conventional OKGI system. Comparing with the conventional OKGI method, the BOKGI method could enhance the sharpness of images and provide a higher spatial resolution of the imaging system. In addition, the influence of the biased angle on the BOKGI performance has been also investigated.

OCIS codes: (190.3270) Kerr effect; (190.7110) Ultrafast nonlinear optics; (300.6530) Spectroscopy, ultrafast; (320.7160) Ultrafast technology; (290.7050) Turbid media.

References and links

1. S. Z. Islam, T. Gayen, B. B. Das, L. Shi, M. Seredych, A. Moussawi, T. J. Bandosz, and R. R. Alfano, "Time-resolved photoluminescence of $Zn(OH)_2$ and its composites with graphite oxides," Opt. Lett. **38**(13), 2227–2229 (2013).
2. C. Calba, L. Méès, C. Rozé, and T. Girasole, "Ultrashort pulse propagation through a strongly scattering medium: simulation and experiments," J. Opt. Soc. Am. A **25**(7), 1541–1550 (2008).
3. S. Idlahcen, C. Rozé, L. Méès, T. Girasole, and J. Blaisot, "Sub-picsecond ballistic imaging of a liquid jet," Exp. Fluids **52**(2), 289–298 (2012).
4. M. Bashkansky, C. L. Adler, and J. Reintjes, "Coherently amplified Raman polarization gate for imaging through scattering media," Opt. Lett. **19**(5), 350–352 (1994).
5. H. Purwar, S. Idlahcen, C. Rozé, D. Sedarsky, and J. B. Blaisot, "Collinear, two-color optical Kerr effect shutter for ultrafast time-resolved imaging," Opt. Express **22**(13), 15778–15790 (2014).
6. T. Fujino, T. Fujima, and T. Tahara, "Picosecond time-resolved imaging by nonscanning fluorescence Kerr gate microscope," Appl. Phys. Lett. **87**(13), 131105 (2005).
7. L. Gundlach and P. Piotrowiak, "Femtosecond Kerr-gated wide-field fluorescence microscopy," Opt. Lett. **33**(9), 992–994 (2008).
8. D. R. Symes, U. Wegner, H. C. Ahlswede, M. J. V. Streeter, P. L. Gallegos, E. J. Divall, R. A. Smith, P. P. Rajeev, and D. Neely, "Ultrafast gated imaging of laser produced plasmas using the optical Kerr effect," Appl. Phys. Lett. **96**(1), 011109 (2010).
9. K. Minoshima, H. Matsumoto, Z. Zhang, and T. Yagi, "Simultanous 3-D Imaging Using Chirped Ultrashort Optical pulse," Jpn. J. Appl. Phys. **33**(9B), L1348–L1351 (1994).
10. T. Yasui, K. Minoshima, and H. Matsumoto, "Three-dimensional shape measurement of a diffusing surface by use of a femtosecond amplifying optical Kerr gate," Appl. Opt. **39**(1), 65–71 (2000).
11. W. Tan, Y. Yang, J. Si, J. Tong, W. Yi, F. Chen, and X. Hou, "Shape measurement of objects using an ultrafast optical Kerr gate of bismuth glass," J. Appl. Phys. **107**(4), 043104 (2010).
12. A. Bassi, D. Brida, C. D'Andrea, G. Valentini, R. Cubeddu, S. De Silvestri, and G. Cerullo, "Time-gated optical projection tomography," Opt. Lett. **35**(16), 2732–2734 (2010).
13. L. Zevallos, E. Manuel, S. K. Gayen, M. Alrubaiee, and R. R. Alfano, "Time-gated backscattered ballistic light imaging of objects in turbid water," Appl. Phys. Lett. **86**(1), 011115 (2005).
14. D. Sedarsky, J. Gord, C. Carter, T. Meyer, and M. Linne, "Fast-framing ballistic imaging of velocity in an aerated spray," Opt. Lett. **34**(18), 2748–2750 (2009).

#223109 - $15.00 USD Received 17 Sep 2014; revised 29 Oct 2014; accepted 30 Oct 2014; published 5 Nov 2014

15. J. B. Schmidt, Z. D. Schaefer, T. R. Meyer, S. Roy, S. A. Danczyk, and J. R. Gord, "Ultrafast time-gated ballistic-photon imaging and shadowgraphy in optically dense rocket sprays," Appl. Opt. **48**(4), B137–B144 (2009).
16. F. X. d'Abzac, M. Kervella, L. Hespel, and T. Dartigalongue, "Experimental and numerical analysis of ballistic and scattered light using femtosecond optical Kerr gating: a way for the characterization of strongly scattering media," Opt. Express **20**(9), 9604–9615 (2012).
17. W. Tan, Z. Zhou, A. Lin, J. Si, P. Zhan, B. Wu, and X. Hou, "High contrast ballistic imaging using femtosecond optical Kerr gate of tellurite glass," Opt. Express **21**(6), 7740–7747 (2013).
18. Q. Z. Wang, X. Liang, L. Wang, P. P. Ho, and R. R. Alfano, "Fourier spatial filter acts as a temporal gate for light propagating through a turbid medium," Opt. Lett. **20**(13), 1498–1500 (1995).
19. L. Wang, P. P. Ho, X. Liang, H. Dai, and R. R. Alfano, "Kerr - Fourier imaging of hidden objects in thick turbid media," Opt. Lett. **18**(3), 241–243 (1993).
20. A. D. Slepkov, F. A. Hegmann, Y. Zhao, R. R. Tykwinski, and K. Kamada, "Ultrafast optical Kerr effect measurements of third-order nonlinearities in cross-conjugated iso-polydiacetylene oligomers," J. Chem. Phys. **116**(9), 3834–3840 (2002).
21. P. Yang, L. Liu, and L. Xu, "Dynamic evolution of light-induced orientation of dye-doped liquid crystals in liquid phase studied by time-resolved optically heterodyned optical Kerr effect technique," J. Chem. Phys. **128**(8), 084710 (2008).
22. H. M. Fan, G. J. You, Y. Li, Z. Zheng, H. R. Tan, Z. X. Shen, S. H. Tang, and Y. P. Feng, "Shape-controlled synthesis of single-crystalline Fe_2O_3 hollow nanocrystals and their tunable optical properties," J. Phys. Chem. C **113**(22), 9928–9935 (2009).
23. M. E. Orczyk, M. Samoc, J. Swiatkiewicz, and P. N. Prasad, "Dynamics of third-order nonlinearity of canthaxanthin carotenoid by the optically heterodyned phase-tuned femtosecond optical Kerr gate," J. Chem. Phys. **98**(4), 2524–2533 (1993).

1. Introduction

Ultrafast imaging provides an interesting tool applied in fields as diverse as medical imaging, fluid dynamics, and material science. The temporal resolution of the ultrafast imaging system is determined by the exposure time of the camera, which can be electronically gated on the timescale of picoseconds [1] and even faster by driving the time gate optically. Until now holography and various nonlinear optics effects, such as second harmonic generation [2, 3], stimulated Raman amplification [4] and the optical Kerr gate (OKG) [5], have been investigated for ultrafast time gating.

An OKG is composed of a pair of crossed polarizers around an isotropic Kerr medium. In an optical Kerr gated imaging (OKGI) system, if there is no gating laser pulse present, the imaging beam passing through the first polarizer will be blocked by the second crossed polarizer (also called analyzer). The imaging beam can pass through the OKG only when an intense, linearly polarized gating laser pulse is introduced into the Kerr medium to induce a transient birefringence, which rotates the polarization of the imaging beam and allows most of it to pass through the analyzer. By using short gating laser pulses and a fast response Kerr medium, it is possible to realize the switch time of the OKG on the timescale of femtoseconds. Comparing with other optical time gate, the OKG has no need of satisfaction of the phase-matching condition and high intensity of the probe light. Therefore, the OKG offers a simple way to operate an ultrafast optical time gate for ultrafast imaging, in which non-scanning two dimensional imaging and wide spectral probe range are possible. Over the past few decades, the OKGI technique has been used widely for ultrafast fluorescence microscope [6, 7], laser produced plasmas diagnosing [8], three-dimensional shape measurements [9–11], time-gated optical projection tomography [12], and imaging of objects hidden in turbid media [13–17].

In the OKGI system, the transient birefringence induced by the gating laser pulse in the isotropic Kerr medium is a nonlinear optical phenomenon, which depends on the laser power intensity. To ensure sufficient signal intensity, the gating beam is usually focused into the Kerr medium. Correspondingly, the imaging beam is firstly focused into the Kerr medium and then re-collimated behind the Kerr medium and finally imaged onto the camera by lenses. As is well-known, a convex lens has inherent ability to perform two-dimensional Fourier transforms. Actually, the imaging beam is firstly Fourier decomposed into different spatial frequency components by the converging lens, which are inverse Fourier transformed to form a true image of the object by the collimating and the imaging lenses. In the process,

#223109 - $15.00 USD Received 17 Sep 2014; revised 29 Oct 2014; accepted 30 Oct 2014; published 5 Nov 2014

the lower spatial components are located at the center portion and the higher spatial components spread away from the lower spatial components. On the other hand, the spatial intensity profile of the gating pulse actually plays the role of a soft aperture in the Kerr medium for the imaging pulse [18]. Therefore, some higher spatial frequency components of the detected object might be filtered by the photo-induced soft aperture, which would reduce the image sharpness, even decrease the spatial resolution of the imaging system. The low-pass filtering would be significantly enhanced, when the Kerr medium is placed on the Fourier plane of the converging lens.

Although placing the Kerr medium on the image plane of the converging lens could avoid the loss of the high spatial frequency components, the object field would be limited by the diameter of the gating laser beam in the image plane [10]. For a big object, the Kerr medium should be placed on the Fourier plane alternatively. Furthermore, to improve the image contrast and signal-to-noise ratio, most OKGI systems for imaging objects hidden in turbid media also place the Kerr medium on the Fourier plane [13, 15, 18, 19]. Since the influence of the low-pass spatial filtering is an intrinsic problem of the OKGI that is not fully resolved, improvements to existing OKGI technique could provide opportunities for the advancement of its capabilities.

In this study, we proposed an improved OKGI technique by using a biased OKG, which was previously applied to probe phase and population effect in molecular systems [20–22]. Our study indicated that the biased OKG was suitable for the application in ultrafast imaging. The experimental results show that by using the biased optical Kerr gated imaging (BOKGI), the high spatial frequency components of the detected object could be effectively retrieved, which are often filtered by the photon-induced soft aperture in a conventional OKGI system. Comparing with the conventional OKGI method, the BOKGI method could enhance the sharpness of images and provide a higher spatial resolution of the imaging system.

2. Principle and experiments

The main experimental arrangement of the biased OKG is similar as that of the conventional OKG, which is also composed of a pair of polarizers around a Kerr medium. However, in the biased OKG, the polarization direction of the output polarizer (also called analyzer) was rotated by a small angle θ away from the orthogonal direction as shown in Fig. 1(a), which was different from the conventional OKG as shown in Fig. 1(b). The polarization directions of the polarizers in the both OKGs were further shown in Fig. 1(c).

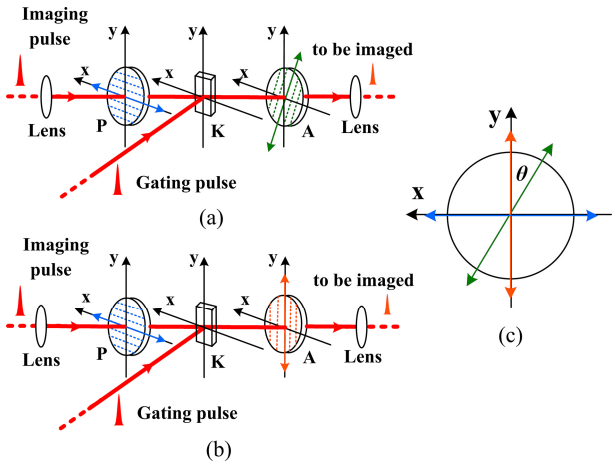

Fig. 1. Schematic diagrams of the biased optical Kerr gate (OKG) and the conventional OKG. P, polarizer; K, optical Kerr medium; A, analyzer. (a) Biased OKG. (b) Conventional OKG. (c) Polarization directions of the analyzers in both of the OKGs. θ is the angle between the polarization directions of the analyzers.

#223109 - $15.00 USD Received 17 Sep 2014; revised 29 Oct 2014; accepted 30 Oct 2014; published 5 Nov 2014

For the biased OKG, the slight rotation of the analyzer creates the optical local oscillator field $E_0\sin\theta$, here E_o is the electric field amplitude of the incident imaging beam. The light electric field amplitude after the analyzer is given by:

$$E \propto E_o \sin\theta + (iF_{\mathrm{Re}} - F_{\mathrm{Im}})\sin\theta + (iH_{\mathrm{Re}} - H_{\mathrm{Im}})\cos\theta \tag{1}$$

Where F and H are the **x** and **y** components of nonlinear optical Kerr response field amplitudes, the subscripts "Re" and "Im" represent their real and imaginary parts, respectively. Since the biased angle θ is limited to a few degrees around 0 and $E_0 >> |F_{\mathrm{Re}}|$, $|F_{\mathrm{Im}}|$, $|H_{\mathrm{Re}}|$, $|H_{\mathrm{Im}}|$, we can disregard the second term $((iF_{\mathrm{Re}}\text{-}F_{\mathrm{Im}})\sin\theta)$ in Eq. (1) and rewrite Eq. (1) as:

$$E \propto E_o \sin\theta + (iH_{\mathrm{Re}} - H_{\mathrm{Im}})\cos\theta \tag{2}$$

Furthermore, taking consideration of $\sin\theta \approx \theta$, $\sin^2\theta \approx 0$, and $\cos^2\theta = 1$, the detected light intensity I after the analyzer can be given by:

$$I \propto H_{\mathrm{Re}}^2 + H_{\mathrm{Im}}^2 - 2\theta E_o H_{\mathrm{Im}} \tag{3}$$

On the right of Eq. (3), the first two terms are the standard optical Kerr signals. In addition, for the biased OKG arrangement, a quarter-wave plate could be optionally inserted in front of the output polarizer to provide a $\pi/2$ phase bias for **x** or **y** components of the light fields. If the optical axis of the quarter-wave plate was parallel to the polarization direction of the input polarizer, the light electric field amplitude E after the analyzer and detected light intensity I would be given by:

$$E \propto E_o \sin\theta + (-H_{\mathrm{Re}} + iH_{\mathrm{Im}})\cos\theta \tag{4}$$

$$I \propto H_{\mathrm{Re}}^2 + H_{\mathrm{Im}}^2 - 2\theta E_o H_{\mathrm{Re}} \tag{5}$$

The detailed theoretical analysis of the biased OKG and its applications on molecular dynamics can be found elsewhere [23]. Here, we focused our attention on the imaging information carried by the biased optical Kerr gated light fields. In the BOKGI system, when the imaging beam passes through the biased OKG, it is firstly Fourier decomposed into different spatial frequency components by the converging lens, which are inverse Fourier transformed to form a true image of the object by the collimating and the imaging lenses. In this process, the biased OKG actually play a crucial role to manipulate the spatial frequency spectrum of the object. Since the nonlinear optical Kerr response fields suffer from the low-pass filtering caused by the photo-induced soft aperture described above, the imaging information carried by the standard optical Kerr signals is the low spatial frequency components of the object. The loss of the high spatial frequency components of the object reduces the image sharpness and the spatial resolution of the imaging system. Unlike the nonlinear optical Kerr response fields, the optical local oscillator field, which is a fraction of the optical electric field of the incident imaging beam, contains all spatial frequency components of the object. So the optical local oscillator field enable effectively retrieve the high spatial frequency components of the object. As a result, the BOKGI performance would be improved as shown in next section of this paper. It should be mentioned that whether the biased angle was positive or negative, the retrieved high spatial frequency components of the detected object might show significantly different imaging performance, which will be also discussed later.

#223109 - $15.00 USD Received 17 Sep 2014; revised 29 Oct 2014; accepted 30 Oct 2014; published 5 Nov 2014

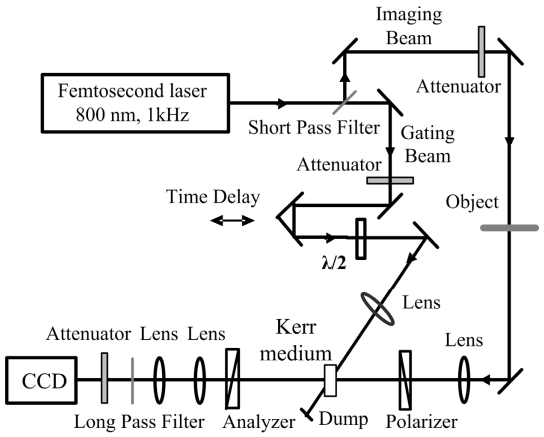

Fig. 2. Schematic of the biased optical Kerr gated imaging system in our experiment.

Figure 2 shows the schematic of the biased optical Kerr gated imaging system in our experiment. The experiments were carried out using femtosecond laser pulses with duration of approximately 50 fs and a center wavelength of 800 nm, emitting from a Ti:sapphire laser system at a repetition rate of 1 kHz. Because the gating pulse might undergo some forward scattering in the Kerr medium and enter the camera to generate significant background noise in the image, a dielectric short-pass filter was used to split the laser beam into two parts. The transmitted part was used as the imaging beam and the reflective part was used as the gating beam, the scattered light of which could be rejected with a long-pass filter. Two neutral attenuators were used to adjust their intensities. The gating beam was optically delayed using a stepper motor resulting in a 0.52 fs/step delay resolution, and then focused into a biased OKG to control its open/close state. A half-wave plate was inserted in the gating beam path to rotate its polarization by $\pi/4$ for the maximum gating efficiency. The imaging beam, passed through a object (United States Air Force test pattern), was then focused into the biased OKG. The carbon disulfide (CS_2) filled in a glass cuvette with a path length of 1 mm was used here as the optical Kerr material and located at the back focal plane of the lens.

When the biased OKG was opened at the zero time delay, after recollimation by a lens behind the analyzer, the imaging beam was detected by CCD camera through another imaging lens. As mentioned above, a long-pass filter was placed before the CCD camera to block noise light caused by the gating beam. Both the short and long wave pass filters have low out-of-band transmittance less than 0.1%. The average transmittance is 80% for the long-pass filter and 65% for the short-pass filter. A neutral attenuator was also used to avoid laser damage on the CCD camera, when the intensity of the gated imaging beam was too strong. In the BOKGI system, the time resolution is limited by either the duration of the laser pulse or the response time of the Kerr medium, whichever is longer. In our experiment, the time resolution of the imaging system has been measured to be about 1.6 ps, which is equal to the molecular relaxation time of the CS_2. Because the images intensity would gradually decrease with increasing the delay time between the gating pulse and the imaging pulse due to the decreased transmittance of the OKG, all the signal images were captured at zero delay time in following discussions. In addition, the images without existence of the gating laser pulse were subtracted from the signal images to remove the remaining leakage through all the filters and the OKG.

3. Results and discussion

To convince the reliability of our biased OKG experimental arrangement, the angular dependence of the BOKGI signals of our imaging system were firstly measured and shown in Fig. 3. The optical axis of the quarter-wave plat was parallel to the polarization direction of the input polarizer. Form Fig. 3, we can see that the BOKGI signals were proportional to the

#223109 - $15.00 USD Received 17 Sep 2014; revised 29 Oct 2014; accepted 30 Oct 2014; published 5 Nov 2014

biased angles. In addition, because the real parts are bigger than the imaginary parts of the nonlinear optical response fields for CS_2 at 800 nm, it also can be seen from Fig. 3 that the BOKGI signals with the quarter-wave plate is bigger than those without the quarter-wave plate at the same biased angle. The experimental results agree well with the biased OKG theory as described in Eqs. (3) and (5). In addition, it should be noted that the BOKGI signal might be negative at the positive biased angle. It can be qualitatively explained as follows. In the BOKGI system, when there is no gating laser pulse present, a fraction of the imaging beam passes through the BOKG and is detected as the biased signal. When the gating laser pulse is introduced into the Kerr medium and induced the transient birefringence, the biased signal will decrease at the positive biased angle and increase at the negative biased angle. Actually, BOKGI signal intensity shown in Fig. 3 is the difference between the biased signal with the gating laser pulse and the biased signal without the gating laser pulse.

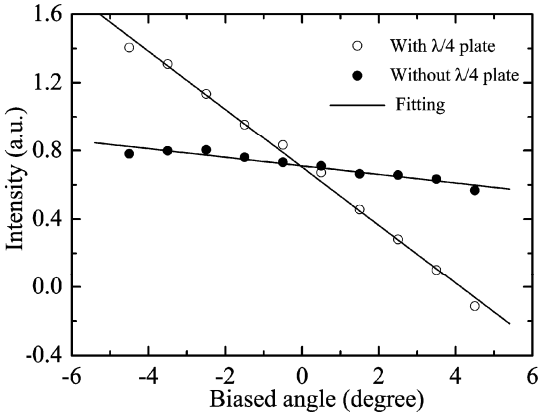

Fig. 3. Angular dependence of the biased OKG signals of the imaging system.

Furthermore, to demonstrate the possible reduction of imaging sharpness for OKGI and the corresponding improvement of imaging quality for BOKGI, some typical images for both OKGI and BOKGI arrangements were photographed and shown in Figs. 4(c) and 4(d), respectively. For comparison, the same images photographed directly and photographed by the spatial filtering imaging arrangement were also shown in Figs. 4(a) and 4(b). For direct imaging arrangement, the Kerr medium was removed and the polarization direction of the analyzer was adjusted to that of the polarizer. For spatial filtering arrangement, the Kerr medium was replaced by a pinhole. The imaging objects were the resolution test patterns, partial sizes of which in white rectangle are shown on the right. From the rows (1) ~(5) of Figs. 4(b) and 4(c), the filtering aperture sizes for SFI are about 1100 μm, 600 μm, 340 μm, 340 μm, and 340 μm, respectively, and the spot diameters (FWHM) at the optical Kerr medium surface of the gating beam are about 1100 μm, 500 μm, 330 μm, 330μm, and 330 μm, respectively.

From rows (1) ~(3) of Fig. 4(b), we can see that the image sharpness decreased with decreasing the pinhole size in SFI system. Similarly, the image sharpness also decreased with decreasing the photo-induced soft aperture in OKGI system as shown in rows (1) ~(3) of Fig. 4(c). Because the size of the photo-induced soft aperture in OKGI system was nearly as big as the pinhole size in SFI system, the experimental results confirmed that the possible reduction of the image sharpness for OKGI was caused by the low-pass filtering effect. Moreover, the low-pass filtering effect could even blur the images with decreasing the object size in OKGI and SFI systems as shown in rows (3) ~(5) of Figs. 4(b) and 4(c), respectively. However, because of effective retrieval of the high spatial frequency components of the object as mentioned above, the image sharpness for BOKGI was almost the same as that for imaging directly as shown in rows (1) ~(5) of Figs. 4(a) and 4(d).

#223109 - $15.00 USD Received 17 Sep 2014; revised 29 Oct 2014; accepted 30 Oct 2014; published 5 Nov 2014

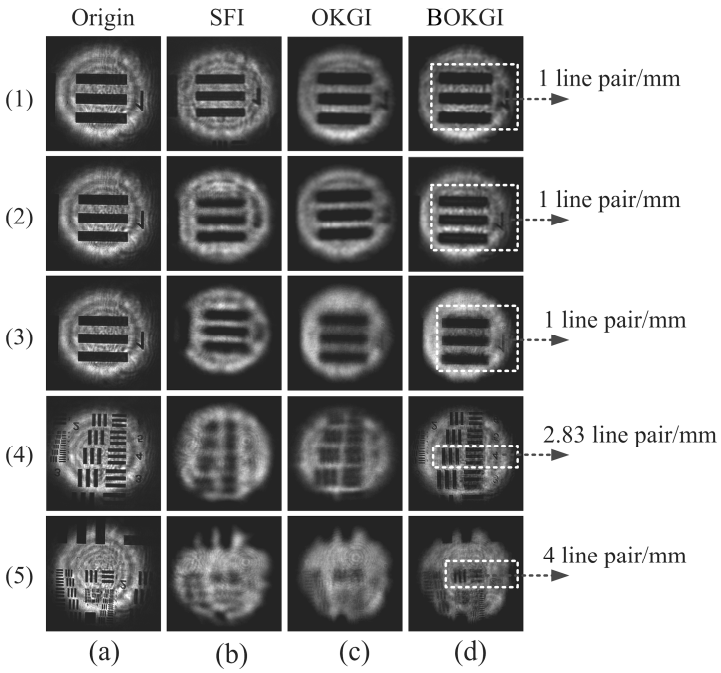

Fig. 4. Comparison of imaging results for four different imaging arrangements. (a) Direct imaging. (b) Spatial filtering imaging (SFI). (c) Optical Kerr gated imaging (OKGI). (d) Biased optical Kerr gated imaging (BOKGI). The imaging object is the resolution test patterns, partial sizes of which are shown on the right. From the row (1) to row (5), the filtering aperture sizes for SFI are about 1100 μm, 600 μm, 340 μm, 340μm, and 340 μm, respectively, and the spot diameters at the optical Kerr medium surface of the gating beam were measured to be about 1100 μm, 500 μm, 330 μm, 330μm, and 330 μm, respectively.

As described in Eqs. (2)-(5), the retrieval of the high spatial frequency components of the object for BOKGI would change with different biased angles and finally affect the BOKGI performance. To further find out the performance of BOKGI at different biased angles, we then photographed some images in BOKGI system at several different biased angles of −1°, −3°, −5°, 1°, 3°, and 5°. Here, the spot diameter (FWHM) at the optical Kerr medium surface of the gating beam was about 330 μm. The objects were some patterns in Group 1 of the resolution test target. The experimental result was shown in Fig. 5(a). For comparison, the same objects were also photographed directly and in OKGI arrangement as shown in Figs. 5(b) and 5(c), respectively.

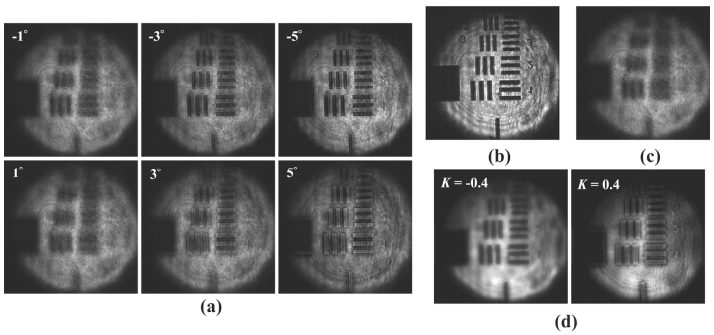

Fig. 5. Comparison of experimental results and simulation for BOKGI at different biased angles. (a) BOKGI at different biased angles. (b) Direct imaging. (c) OKGI. (d) Simulation of BOKGI at different biased angles.

#223109 - $15.00 USD Received 17 Sep 2014; revised 29 Oct 2014; accepted 30 Oct 2014; published 5 Nov 2014

From the first row of Fig. 5(a), we can see that when the biased angles are negative, the image sharpness increases with increasing the biased angles. At biased angle −5°, the image sharpness for BOKGI is nearly the same as that for imaging directly shown in Fig. 5(b). However, from the second row of Fig. 5(a), we can see that when the biased angles are positive, the images do not only increase sharpness with increasing the biased angles, but also gradually show an unnatural reversed contrast of the resolution test patterns. This can be explained as follows.

When the biased angles were negative, the retrieved high spatial frequency components were in phase with the low spatial frequency components in the spatial frequency domain according to Eqs. (2) and (4). In this case, the light fields after the biased OKG have the similar spatial frequency components as those the incident imaging beam carried, except that they have different amplitude ratios between the high and the low spatial frequency components. So when the biased angles were negative, the image sharpness increased with increasing the biased angles due to the gradually enhanced retrieval of the high spatial frequency components of the object. However, when the biased angles were positive, the retrieved high spatial frequency components were out of phase with the low spatial frequency components. Depending on the proportion of the inverted-phase high spatial frequency components in the whole spatial frequency components of the object, the object image might show the unnatural reversed contrast as shown in the second row of Fig. 5(a). A schematic simulation was further performed to prove the inference, in which Fig. 5(b) was used as the input image. In the simulation, the input image was firstly Fourier decomposed into different spatial frequency components ($\mathcal{F}\{E\}$). A Gauss filter function was used to pick up the low ($\mathcal{F}\{E\}_{\text{low}}$) and the high frequency components ($\mathcal{F}\{E\}_{\text{high}}$). To simulate the influence of different biased angles on the imaging performance, the $\mathcal{F}\{E\}_{\text{low}} - K\mathcal{F}\{E\}_{\text{high}}$ was used as the final frequency components and then inverse Fourier transformed to form the simulated images, where, $-1 < K < 1$. Figure 5(d) shows two typical simulated images, in which K was set to be −0.4 and 0.4 to simulate the negative and positive biased angles. From Figs. 5(a) and 5(d), we can see that the simulation agrees well with the experimental results and confirms our explanations above.

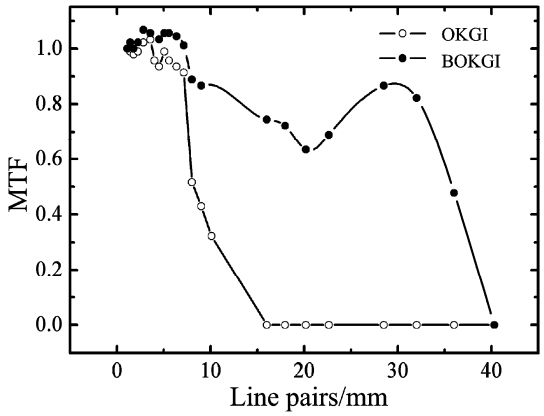

Fig. 6. Comparison of the modulation transfer function (MTF) of the BOKGI and the OKGI systems.

To quantitatively compare the performance of the OKGI and the BOKGI systems, we further evaluated the modulation transfer function (MTF) of both imaging systems according to MTF = $Contrast_i$ / $Contrast_{ref}$, where $Contrast = (I_{max} - I_{min}) / (I_{max} + I_{min})$. The $Contrast_i$ represents the contrast for a resolution test pattern measured, i denotes its spatial frequency, I_{max} is the average light intensity corresponding to the unshadowed region of the imaged resolution chart, and I_{min} is the average light intensity corresponding to the shadowed region.

#223109 - $15.00 USD Received 17 Sep 2014; revised 29 Oct 2014; accepted 30 Oct 2014; published 5 Nov 2014

In addition, the reference contrast $Contrast_{ref}$ was determined by the contrast of the resolution test pattern with lowest spatial frequency in the image. Here, $Contrast_{ref} = Contrast$ (1.12 lp/mm (line pairs per millimeter)). From Fig. 6, we can see that the MTF value for BOKGI is higher than that for OKGI for a same resolution test pattern. In addition, the cutoff spatial frequency of the BOKGI system is 40 lp/mm and gives a spatial resolution of 12.5 μm. Comparing with the BOKGI system, the cutoff spatial frequency of the OKGI system reduced to 16 lp/mm with a resolved object size of 31.25 μm. These results indicate that the performance of the imaging system can be effectively improved by using the biased OKG than that by using the conventional OKG. It should be also noted that although the BOKGI can enhance the sharpness of images and provide a higher spatial resolution of the imaging system, the BOKGI at a big biased angle would cause a reduction in the signal dynamic range. Thus a small biased angle (< 5°) was used in out experiment.

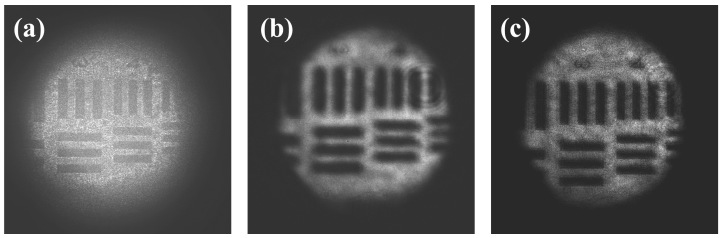

Fig. 7. Images of the resolution test patterns behind a turbid medium for different imaging methods. (a) Direct imaging. (b) OKGI. (d) BOKGI.

As one of the potential applications, we finally demonstrated to image an object hidden behind turbid medium by using the BOKGI method. Some resolution test patterns were selected as the imaging objects and a dense suspension of 3.13-μm-diameter polystyrene microspheres was used as the turbid medium. Figure 7(a) shows a disturbed image of the objects by imaging directly. From Fig. 7(a), we can see that the image contrast decreases due to the scattering noise photons. Figures 7(b) and 7(c) show the images of the objects by the OKGI and the BOKGI, respectively. From Figs. 7(b) and 7(c), we can see that comparing with the OKGI, the BOKGI does not only increase the visualization of the objects, but also increases the image sharpness.

4. Conclusion

In summary, we proposed a BOKGI method for ultrafast imaging. The performance of the BOKGI system has been investigated. Experimental results showed that by using the BOKGI, the high spatial frequency components of the detected object could be effectively retrieved, which are often filtered by the photon-induced soft aperture in a conventional OKGI system. Comparing with the conventional OKGI method, the BOKGI method could enhance the sharpness of images and provide a higher spatial resolution of the imaging system. In addition, the BOKGI with positive biased angles did not only show increased image sharpness with increasing the biased angles, but also gradually exhibited an unnatural reversed contrast compared with the BOKGI with negative biased angles. This phenomenon was attributed to the different phase between the high and the low spatial frequency components of the object, which were carried by the biased optical Kerr gated imaging beam. In the end, the BOKGI for objects hidden behind turbid medium has been demonstrated to give an example of its applications.

Acknowledgments

The authors gratefully acknowledge the financial support for this work provided by the National Natural Science Foundation of China under the Grant Nos. 61235003, 61308036 and 61205129, the Fundamental Research Funds for the Central Universities (Grant No. xjj2012020), the China Postdoctoral Science Foundation funded project (2013M540753), and Opened Fund of the State Key Laboratory on Integrated Optoelectronics No. IOSKL2012KF.

#223109 - $15.00 USD Received 17 Sep 2014; revised 29 Oct 2014; accepted 30 Oct 2014; published 5 Nov 2014